ACS Catalysis

Research Article

pubs.acs.org/acscatalysis

Remedying Defects in Carbon Nitride To Improve both Photooxidation and H_2 Generation Efficiencies

Wenting Wu,[†,‡] Jinqiang Zhang,[†] Weiyu Fan,[†] Zhongtao Li,[†] Lizhuo Wang,[†] Xiaoming Li,[‡] Yang Wang,[†] Ruiqin Wang,[†] Jingtang Zheng,[†] Mingbo Wu,*[,†] and Haibo Zeng*[,‡]

[†]State Key Laboratory of Heavy Oil Processing, School of Chemical Engineering, China University of Petroleum, Qingdao 266580, People's Republic of China

[‡]Institute of Optoelectronics & Nanomaterials, Herbert Gleiter Institute of Nanoscience, School of Materials Science and Engineering, Nanjing University of Science and Technology, Nanjing 210094, People's Republic of China

Supporting Information

ABSTRACT: The outstanding visible light response of carbon nitride has aroused intense expectations regarding its photocatalysis, but it is impeded by the inevitable defects. Here, we report on a facile melamine-based defect-remedying strategy and resultant carbon nitride high-performance photocatalysts (R-C_3N_4). Melamine with amino groups and a triazine structure was selected as a "little patch" to passivate and remedy various defects inside carbon nitride. Such a remedying effect has been comprehensively proven by Fourier transform infrared spectroscopy (FT-IR), X-ray photoelectron spectroscopy (XPS), transmission electron microscopy (TEM), scanning electron microscopy (SEM), X-ray diffraction (XRD) analyses, and the ninhydrin test. In addition, their effects on photocatalysis were also individually confirmed by chemical methods, including cyano reduction reactions and deamination reactions. Furthermore, melamine remediation can result in g-C_3N_4/mpg-C_3N_4 junctions, which also favors electron transfer and charge separation during the photocatalytic reaction. In order to explore its broader applications, R-C_3N_4 was used as a photocatalyst for the photooxidation reaction of 1,4-dihydro-2,6-dimethylpyridine-3,5-dicarboxylate (1,4-DHP) and simultaneous H_2 evolution. The conversion rates of 1,4-DHP and H_2 production catalyzed by R-C_3N_4 were enhanced 2 and 6.5 times, respectively. This rational design is beneficial for the conversion of 1,4-DHP during the preparation of bioactive compounds and clean hydrogen production at the same time.

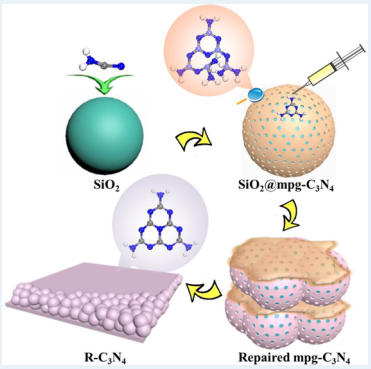

KEYWORDS: *carbon nitride, defect, remedy, photooxidation, H_2 evolution*

INTRODUCTION

Visible light photocatalysis has inspired great interest, offering a sustainable pathway to drive a series of photooxidation reactions, water splitting, and so on.[1−8] The search for highly active and low-cost photocatalysts has been a continuing worldwide endeavor.[1−8] Wide band gap semiconductors such as ZnO and TiO_2 have been explored a great deal, but their main issue is that the photocatalytic response is mainly initiated in the near-UV or UV region to execute the photocatalytic behavior. Thus, the presence of a UV light source is necessary.[9,10] The emergence of organic semiconductors, such as polymeric carbon nitride (C_3N_4), provides a new chance for the development of high-performance photocatalysts in the visible light region.[11−18] Many efforts have been employed to enhance their photocatalytic activity, such as metal/nonmetal doping,[19,20] surface heterojunction design,[19,21] texture and morphology engineering,[22−24] etc. The surface area and photocatalytic ability have been improved significantly; however, the accompanying disordered structure caused a large amount of defects in the final product.[25,26] In addition, these structure defects extremely limit electron−hole separation and transport, which are key rate-determining steps in the photocatalysis.[27]

In essence, among various precursors (e.g., cyanamide, dicyandiamide, thiourea, and urea), the amino and cyano groups are not only crucial functional groups for the chemosynthesis of carbon nitride but also the strongest electron donors/acceptors, which play important roles in the electron−hole separation.[28] As typical groups, they deserve to be studied in detail. Furthermore, mesoporous carbon nitride (mpg-C_3N_4) prepared from cyanamide (only amino and cyano groups) is a good candidate for a defect study.[29] Conventional methods with high calcination temperature could reduce the amount of defects, but the higher temperature also could decompose C_3N_4, reducing the product yield.[30] Calcination under H_2 or NH_3 is limited for the amino defects.[31,32] Thus, it is highly desired to repair various defects and understand their structure−property relationship, especially for the defects of amino and cyano groups. Due to the difficulty in defect characterization, little information is available on the effects of

Received: March 25, 2016
Published: April 6, 2016

DOI: 10.1021/acscatal.6b00879
ACS Catal. 2016, 6, 3365−3371

these defects on the photocatalysis performance of carbon nitride materials.

Herein, we report a facile and comprehensive defect repair and its robust performance in photooxidation and H_2 evolution. Melamine with amino groups and a triazine structure has been selected as a functionalized "little patch" to react with various defects[30] and elaborately remedy them; this was confirmed by Fourier transform infrared spectroscopy (FT-IR), X-ray photoelectron spectroscopy (XPS), transmission electron microscopy (TEM), scanning electron microscopy (SEM), X-ray diffraction (XRD) analyses, and the ninhydrin test. In addition, the "little patch" easily forms nanosheet g-C_3N_4, which shows a CB/VB value higher than that of mpg-C_3N_4. In addition to the fewer defects, the formation of a homojunction structure could improve the electron transfer and charge separation.[19,33] In order to explore its broader applications, R-C_3N_4 was used as a photocatalyst for the photooxidation reaction of 1,4-dihydro-2,6-dimethylpyridine-3,5-dicarboxylate (1,4-DHP) and simultaneous H_2 evolution.[34] The effects of defects on photooxidation were individually confirmed by chemical methods. The conversion rates of 1,4-DHP and H_2 evolution catalyzed by R-C_3N_4 were enhanced 2 and 6.5 times, respectively. This rational design could be beneficial for the conversion of 1,4-DHP during the preparation of bioactive compounds[34] and clean hydrogen production at the same time.

EXPERIMENTAL SECTION

Materials Synthesis. mpg-C_3N_4 and g-C_3N_4 were prepared by methods previously reported.[24] R-C_3N_4 was repaired via a facile copolymerization method. Cyanamide was dissolved in a 40% dispersion of 12 nm SiO_2 particles (Ludox HS40, Aldrich) in water with stirring at 333 K overnight. Then the resulting transparent mixtures were completely ground and mixed with various amounts of melamine (25%, 37.5%, or 50%). The ground mixtures were then heated at a rate of 2.3 K/min over 4 h to reach a temperature of 823 K and tempered at this temperature for another 4 h. The resulting powder was treated with 4 M NH_4HF_2 for 24 h to remove the hard template. The powders were then centrifuged and washed three times with distilled water and twice with ethanol. Finally the powders were dried overnight at 343 K under vacuum. For comparison, the amount of melamine (25%, 37.5% ,and 50%) was set as the parameter for ensuring the optimum result. When the ratio of melamine to mpg-C_3N_4 prepolymer reaches 37.5%, R-C_3N_4 shows the least defects and excellent electron−hole separation and transfer properties. Thus, in this work, the ratio of melamine to mpg-C_3N_4 prepolymer was 37.5%.

Measurement and Characterization. The structures and morphologies of the samples were characterized by X-ray diffraction (XRD) (X'Pert PRO MPD, Holland), scanning electron microscopy (SEM) (Hitachi S-4800, Japan), and transmission electron microscopy (TEM) (JEM-2100UHR, Japan). The functional groups in the samples were characterized by Fourier transform infrared spectrometry (FTIR) (Thermo Nicolet NEXUS670, USA). Further evidence for the composition of the product was inferred from X-ray photoelectron spectroscopy (XPS), using an ESCALAB 250Xi spectrometer equipped with a prereduction chamber. Elemental analysis was detected by an Elementar Vario EL III instrument (Elementar, Germany). The UV−vis diffuse reflection spectra were obtained for the dry-pressed disk samples using a Scan UV−vis spectrophotometer (UV−vis DRS UV-2450, Shimadzu, Japan) equipped with an integrating sphere assembly, using $BaSO_4$ as a reflectance sample. Nitrogen adsorption−desorption isotherms were obtained on a nitrogen adsorption apparatus (Micromeritics ASAP 2020M) with all samples degassed at 423 K for 12 h prior to measurements.

Ninhydrin Test.[35] The ninhydrin test was performed by adding 1 mL of ninhydrin acetone solution (80 mg/mL) to 2 mL of a C_3N_4 suspension (C_3N_4, 2.0 mg) and then heating the covered mixture in a boiling water bath for 15 min. The UV−vis absorption spectra were measured with a UV−vis spectrometer directly using the solution after heating; the absorption intensity quantitatively indicates the amount of NH_2 or NH in the C_3N_4.

Cyano Reduction Reaction.[36] $NaBH_4$ (19.0 mg, 0.5 mmol) was dissolved in dry THF (10 mL), 10 mL of a trifluoroacetic acid (TFA) solution in THF (0.01 M) was injected into the $NaBH_4$ solution drop by drop, and then 100.0 mg of mpg-C_3N_4 was added. The suspension was stirred overnight. Finally, the reaction was quenched by 10 mL of water. The reduced mpg-C_3N_4 was filtered and washed four times, and then dried at 60 °C in the vacuum oven overnight.

$$X{-}CN \xrightarrow{NaBH_4} X{-}C{-}NH_2$$

Preparation of Deaminated C_3N_4. A 100.0 mg portion of mpg-C_3N_4 was added to 40 mL of dilute HCl at 5−10 °C. A 10 mL amount of an $NaNO_2$ solution (0.05 M) was slowly added to the suspension over 5 h. Then a hypophosphorous acid solution (1.0 g, 50%) was added to the mixture mentioned above. The mixture was stirred overnight. Finally, the deaminated mpg-C_3N_4 was filtered and washed four times and dried overnight at 60 °C in the vacuum oven.

$$X{-}NH_2 \xrightarrow{HNO_2} X{-}N{\equiv}N^+ \xrightarrow{H_3PO_2} X{-}H$$

Electrochemical Analysis.[37] The photocurrent measurement and electrochemical impedance spectroscopy (EIS) experiments were conducted using an Ametek PARSTAT4000 electrochemistry workstation using a standard three-electrode cell with a working electrode, a platinum counter electrode, and a Ag/AgCl reference electrode. The working electrodes were prepared as an indium tin oxide glass (ITO) decorated with catalyst samples. In a typical procedure, 30.0 mg of photocatalyst was first dispersed in 2 mL of acetone containing polyvinylidene fluoride (PVDF) solution (50 μL, 5 wt %); the slurry was then spread onto the ITO. After air drying, the electrode was annealed at 573 K for 30 min in air to improve the adhesion. Na_2SO_4 (0.5 M) was used as the electrolyte solution. Visible light irradiation was provided by a 300 W Xe lamp with a cutoff filter (Kenko L-42). The exposed area under illumination was 1 cm^2. For electrochemical impedance spectroscopy (EIS) experiments, the perturbation signal was 10 mV and the frequency ranged from 100 kHz to 10 mHz.

Photooxidation of 1,4-DHP. The photochemical reaction was performed at room temperature in an air atmosphere in a two-neck round-bottom flask (25 mL) with irradiation by a 35 W xenon lamp. The aqueous solution (20 mL) containing 10^{-4} mol/L of 1,4-DHP and photocatalysts (20.0 mg) was irradiated at λ >420 nm. This reaction was monitored by UV−vis spectroscopy, and absorption changes were recorded at intervals of 10 min.

Hydrogen Production. The photocatalytic activity of the as-repaired R-C_3N_4 was also evaluated by the photocatalytic oxidation of 1,4-DHP to produce H_2 from acetonitrile solutions. The H_2 evolution test was performed by using a

DOI: 10.1021/acscatal.6b00879
ACS Catal. 2016, 6, 3365−3371

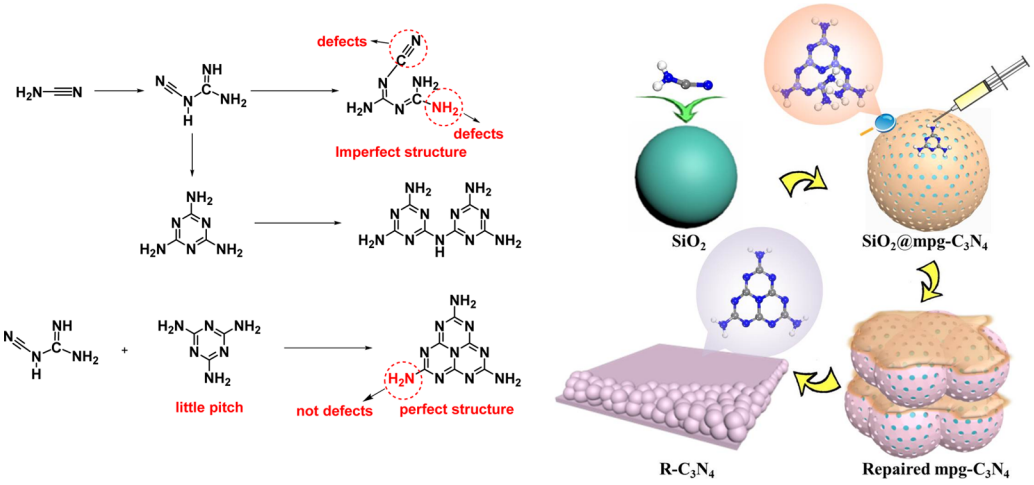

Figure 1. Schematic illustration of repairing defects of mpg-C_3N_4 to R-C_3N_4.

LabSolar-III AG reaction cell (Beijing PerfectLight Co.). 1,4-DHP (100.0 mg, 0.4 mmol), 30 mg of the photocatalyst, and $(NH_4)_2PtCl_6$ (0.5 mg, 0.001 mmol) were dissolved in 40 mL of acetonitrile in a Pyrex reactor. The suspension was thoroughly degassed to remove air and irradiated using a 300 W Xe lamp (PLS-SEX300/300UV, Beijing PerfectLight Co.). A cutoff filter (Kenko L-42) was employed to achieve visible-light (λ >420 nm) irradiation. The yield of H_2 was determined by using an online gas chromatograph (GC7900, Techcomp) equipped with a column of 5 Å molecular sieves and a thermal conductivity detector, and Ar was used as the carrier gas.

Electron Spin Resonance (ESR) Spectroscopy. For the ESR detection of superoxide anion radicals ($O_2^{\bullet-}$), ESR samples were injected into a quartz capillary in darkness and illuminated in the cavity of the ESR spectrometer. Photosensitizers and 5,5-dimethyl-1-pyrroline *N*-oxide (DMPO, superoxide anion radical $O_2^{\bullet-}$ scavenger) in an air-saturated aqueous solution were stirred in the dark, and then the solution was injected into the quartz capillary. A diode-pumped solid state (DPSS) laser (532 nm) was used for the photoirradiation of the solution in the quartz capillary for 100 s.

RESULTS AND DISCUSSION

Comprehensive Repairing Strategy for Various Defects. Due to the lack of purification steps after synthesis, there are many unreacted amino/cyano groups, and other relative intermediates are involved in the photocatalysis application. The final products are hard to purify, and defects are inevitable in the photocatalysis application. Actually, these various defects could be repaired through a facile copolymerization with a functionalized "little patch" (Figure 1). Melamine is composed of amino groups and a triazine structure. The amino group could react with amino/cyano defects and their relative intermediates to repair these defects.[32,38] The triazine structure has a π conjugation, which benefits electron transfer. Thus, melamine is a good "little patch" candidate for mpg-C_3N_4.

First, a prepolymer of mpg-C_3N_4 was obtained through cyanamide cladding of the silicon dioxide pellets. Next, melamine as a functionalized "little patch" was mixed with the prepolymer of mpg-C_3N_4 and polymerized together at high temperature. During the copolymerization process, amino groups of melamine could repair or passivate defects of mpg-C_3N_4. Finally, R-C_3N_4 could be obtained by removing the silica template. In order to ensure the repair optimum, the amount of melamine (25%, 37.5%, and 50%) was set as the parameter. When the weight ratio of melamine to the total of cyanamide and melamine reaches 37.5%, R-C_3N_4 shows the least amount of defects and excellent electron−hole separation and transfer properties (vide infra). Thus, in this work, the weight ratio of melamine was 37.5% in the following.

Characterization of the Repair for mpg-C_3N_4. As shown in the TEM and SEM images (Figure 2 and Figure S1 in the Supporting Information), the as-synthesized R-C_3N_4 is coated by the nanosheet g-C_3N_4. In comparison with TEM images of g-C_3N_4 and mpg-C_3N_4, R-C_3N_4 is composed of mpg-C_3N_4 and exfoliated g-C_3N_4, and this laminar morphology looks like a silk veil on the mpg-C_3N_4 to smooth and repair the defects of mpg-C_3N_4. X-ray diffraction (XRD) patterns also confirm the results mentioned above (Figure 2d). They show obvious signals at 2θ = 27.48° (d = 0.326 nm), which originate from the (002) interlayer diffraction of a carbon nitride graphitic-like structure.[39] In comparison with g-C_3N_4, the (002) diffraction of R-C_3N_4 is significantly weakened, indicating a nanosheet structure on the surface of R-C_3N_4.[40,41] Thus, the surface area of R-C_3N_4 (231.3 m^2 g^{-1}) is spontaneously larger than those of other species (221.3 and 16.9 m^2 g^{-1}) (Figure S2 and Table S1 in the Supporting Information).

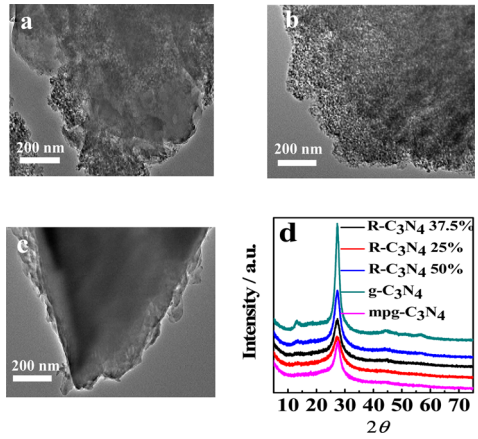

Figure 2. TEM images of (a) R-C_3N_4, (b) mpg-C_3N_4 and (c) g-C_3N_4. (d) XRD patterns of mpg-C_3N_4, R-C_3N_4, and g-C_3N_4.

DOI: 10.1021/acscatal.6b00879
ACS Catal. 2016, 6, 3365−3371

Cyano defects exist in an imperfect structure, which can be seen in Figure 1. Fourier transform infrared (FT-IR) spectra were measured to determine the repair of cyano defects. FT-IR spectra of the as-prepared C_3N_4 from cyanamide shows different intensities around 2150 cm^{-1} (Figure 3a). This peak

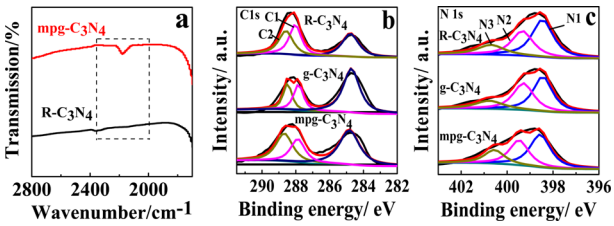

Figure 3. (a) FT-IR spectra of mpg-C_3N_4 and R-C_3N_4. (b, c) High-resolution C 1s and N 1s XPS spectra for R-C_3N_4, mpg-C_3N_4, and g-C_3N_4.

is attributed to cyano terminal groups C≡N (major defects). The cyano peak can be clearly observed in mpg-C_3N_4. On the introduction of melamine into R-C_3N_4, the peak at 2150 cm^{-1} almost disappears, implying that the cyano defects of R-C_3N_4 have been successfully repaired.

Amino groups in the imperfect structure are also other typical defects (Figure 1). X-ray photoelectron spectroscopy (XPS) was employed to accurately measure the chemical bonding of the samples and amino groups. Herein, these amino groups include amino defects and amino groups from a perfect triazine structure (not amino defects). Figure 3b,c shows the typical C 1s and N 1s peaks in the XPS spectra of the as-prepared C_3N_4, which confirm the decrease of amino groups mentioned above. The 288.0 eV peak for C−N bonds in the C 1s spectra could be further deconvoluted into 287.9 eV (C1) and 288.4 eV (C2), which are attributed to the sp^2-hybridized carbon bonded to N inside the triazine rings (C═N) and the sp^2-hybridized carbon bonded to the $-NH_2$ group (═C−NH_2), respectively. To some extent, the ratio of C2 to C1 indicates the degree of depolymerization and the amount of amino groups. mpg-C_3N_4 shows the highest ratio of C2 to C1 (1.19), followed by g-C_3N_4 (1.04). After repair with melamine, R-C_3N_4 shows the lowest ratio of C2 to C1 (0.82), indicating that R-C_3N_4 has a higher polymerization degree and fewer amino groups. Similar results were also observed through N 1s spectra. The N 1s spectra can be deconvoluted into ∼398.7 eV (N1), 399.5 eV (N2), and 400.7 eV (N3), which correspond to sp^2 N atoms involved in triazine rings (C═N), N atoms in H−N−$(C)_2$, and C−NH_2, respectively. The ratio of the sum of N2 and N3 to N1 indicates the degree of depolymerization. mpg-C_3N_4 shows the highest ratio (1.46), followed by g-C_3N_4 (1.30), R-C_3N_4 has the lowest ratio (1.17). These values are consistent with the results obtained from the C 1s spectra and elemental analysis (Table S2 in the Supporting Information).

In order to further identify the amino defects, the ninhydrin test was employed to measure the concentration of amino defects on the surface of these samples. Ninhydrin (2,2-dihydroxyindane-1,3-dione) can only react with amino defects without the interference of other NH_2/NH groups in a perfect triazine structure.[42] Subsequently it produces "Ruhemann's purple", which can be detected at 570 nm in UV−vis absorption spectra.[35] The absorption intensity quantitatively indicates the amount of the amino defects in carbon nitride. As can be seen from Figure 4a, the intensity of R-C_3N_4 is only two-thirds that of mpg-C_3N_4, which is consistent with XPS results.

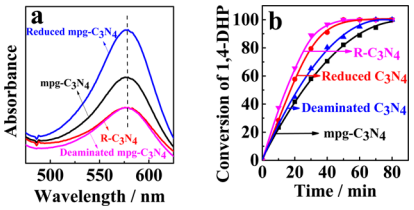

Figure 4. (a) Optical absorption spectra of the solutions from ninhydrin tests. (b) Photooxidation conversion of 1,4-DHP using different samples on the basis of the same procedure.

Therefore, the amino defects were also well repaired through this simple copolymerization method.

Optical and Electrical Properties of R-C_3N_4. It should be noted that the repair of mpg-C_3N_4 with melamine is not merely a simple physical mixing process. The surface of R-C_3N_4 repaired by nanosheet g-C_3N_4 became smooth, which could be confirmed by the relatively weaker absorption intensity of R-C_3N_4 (Figure S3 in the Supporting Information). Meanwhile, it could produce a close isotype homojunction, providing an electron−hole separate transfer route in the isotype homojunctions of g-C_3N_4 and mpg-C_3N_4.[19,43] The band structures of g-C_3N_4 and mpg-C_3N_4 were examined by valence-band (VB) XPS and band gap energies (Figure 5). On the basis of VB XPS,

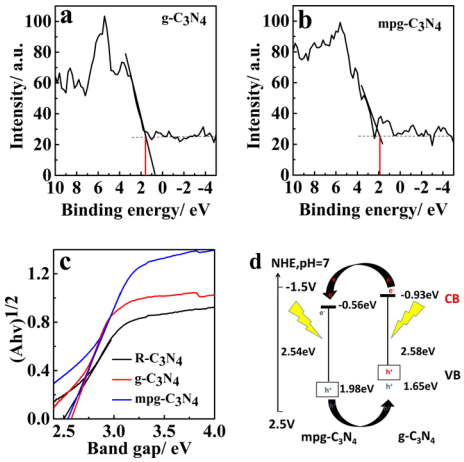

Figure 5. (a, b) VB (valence band) XPS of mpg-C_3N_4 and g-C_3N_4. (c) UV−vis diffuse reflection spectra of mpg-C_3N_4, R-C_3N_4 and g-C_3N_4. (d) Electron transfer mechanism in the g-C_3N_4/mpg-C_3N_4 homojunction.

the VB maxima of g-C_3N_4 and mpg-C_3N_4 are 1.65 and 1.98 V versus NHE, respectively. The VB potential of mpg-C_3N_4 is 0.33 V more positive than that of g-C_3N_4, which can drive the migration of photoinduced holes (h^+) from mpg-C_3N_4 to g-C_3N_4. In combination with the band gap energies, the CB potentials of g-C_3N_4 and mpg-C_3N_4 are calculated to be −0.93 and −0.56 V, respectively, indicating that the CB potential of g-C_3N_4 is 0.37 V more negative than that of mpg-C_3N_4. The CB offset between g-C_3N_4 and mpg-C_3N_4 can drive the migration of photogenerated electrons (e^-) from g-C_3N_4 to mpg-C_3N_4. Thus, electrons are redistributed on the mpg-C_3N_4 side of the junction, and the holes are located on the opposite side (g-C_3N_4), which greatly reduces the energy-wasteful electron−hole recombination (Figure 5d).

To analyze the generation of unpaired electrons and hols in the photocatalyst, as-prepared carbon nitrides were measured

DOI: 10.1021/acscatal.6b00879
ACS Catal. 2016, 6, 3365−3371

by ESR spectroscopy at room temperature, as shown in Figure 6a. The tensor parameter (g) is 2.0020, which could be

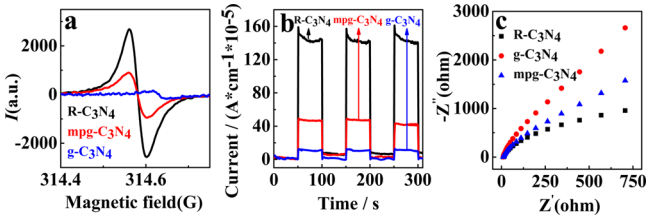

Figure 6. (a) ESR spectra of g-C_3N_4, mpg-C_3N_4, and R-C_3N_4. (b) Photoresponses of g-C_3N_4, mpg-C_3N_4, and R-C_3N_4. (c) Nyquist plots for g-C_3N_4, mpg-C_3N_4, and R-C_3N_4 electrodes under visible light irradiation (λ >420 nm, [Na_2SO_4] = 0.5 M).

attributed to the unpaired electrons on π-conjugated carbon nitride aromatic rings.[21] In comparison with g-C_3N_4 and mpg-C_3N_4, R-C_3N_4 shows a much stronger signal for the unpaired electrons, indicating that repair with a functionalized "little patch" has improved the efficiency of electron−hole separation in the photocatalyst. Furthermore, Figure 6b shows the transient photocurrent responses via three on−off cycles of g-C_3N_4, mpg-C_3N_4, and R-C_3N_4 electrodes, which directly correlate with the separation efficiency of photogenerated electrons and holes. It can be clearly seen that these samples give photocurrents with good reproducibility under visible light, indicating that the carbon nitride electrodes are stable and the photoresponses are reversible. The visible irradiated photocurrent density of R-C_3N_4 is nearly 4.0 times that of mpg-C_3N_4. Electrochemical impedance spectrosscopy (EIS) was also studied, as shown in Figure 6c. R-C_3N_4 shows a smaller arc radius in the EIS Nyquist plot, suggesting less interface electron resistance. Therefore, the repair of mpg-C_3N_4 with a functionalized "little patch" has enhanced photoinduced electron−hole separation and conductivity of carbon nitride, which also benefit electron transfer in both the photoxidation reaction and H_2 generation.

Application of R-C_3N_4 to the Photooxidation and H_2 Evolution from 1,4-DHP. To confirm the photocatalytic abilities of mpg-C_3N_4 after repair, the photooxidation of 1,4-DHP was carried out, which was irradiated in an air atmosphere instead of a pure oxygen atmosphere. As shown in Figure S4 in the Supporting Information, upon irradiation of the mixed solution of photocatalyst and 1,4-DHP with a xenon lamp, the absorption of 1,4-DHP at 374 nm decreased and the absorption of the product (pyridine derivatives, **1b**) at 280 nm increased, which was demonstrated by the changes in UV curves. After the reaction photocatalyzed by R-C_3N_4, the product **1b** was obtained by simple filtration without further purification. Figure 7a,b shows that the efficiency of photocatalytic oxidation in R-C_3N_4 is nearly 2 times that of mpg-C_3N_4 and almost 5 times that of g-C_3N_4. Either no R-C_3N_4 or no light was used for blank experiments; there was no obvious decrease in the absorption at 374 nm, indicating no conversion of 1,4-DHP. To further underline the necessity of excellent interconnection for R-C_3N_4, a physically mixed sample of mpg-C_3N_4 and g-C_3N_4 was also tested for photocatalytic activity, and no significant enhancement could be observed (Figure S4). Figure 7c shows the durability of R-C_3N_4 for photocatalytic oxidation of 1,4-DHP. After three consecutive operations, the efficiency remains stable without noticeable deactivation.

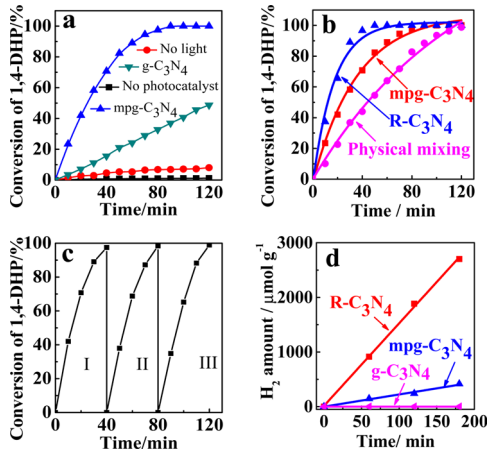

Figure 7. (a, b) Comparison of the conversion of 1,4-DHP among R-C_3N_4, g-C_3N_4, and mpg-C_3N_4. (c) Durability of R-C_3N_4 in the photooxidation of 1,4-DHP. (d) Amount of H_2 produced by R-C_3N_4 and mpg-C_3N_4.

In order to further enhance the atom economy, R-C_3N_4 was applied to hydrogen evolution with 1,4-DHP and $(NH_4)_2PtCl_6$ in the absence of oxygen. As shown in Figure 7d, R-C_3N_4 exhibits superior H_2 evolution (2700 μmol/g). Meanwhile, the turnover number (TON, over a platinum cocatalyst) of R-C_3N_4 is 2400, 6.5 times faster than that of mpg-C_3N_4 (TON 368; Table S1 in the Supporting Information). No H_2 evolution was detected in the g-C_3N_4 system because of the low photocatalytic performance. The R-C_3N_4 performance in H_2 evolution is better than that of photooxidation (2 times). This further indicates the importance of the defect repair.

Mechanism of Photooxidation and H_2 Evolution. The mechanism of the photooxidation for 1,4-DHP is shown in Figure 8a. The electron−hole separation and transfer are crucial

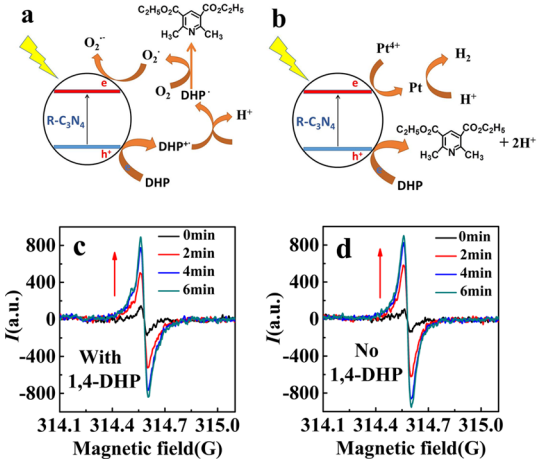

Figure 8. (a) Mechanism for the photooxidation of 1,4-DHP with R-C_3N_4 in the presence of O_2. (b) Mechanism for the H_2 evolution from 1,4-DHP in the absence of O_2. (c) ESR spectra of R-C_3N_4 with 1,4-DHP. (d) ESR spectra of R-C_3N_4 without 1,4-DHP.

for the photocatalysis. In order to confirm the mechanism, electron spin resonance (ESR) spectroscopy was employed with 5,5-dimethyl-1-pyrroline *N*-oxide (DMPO) as a scavenger for $O_2^{\bullet-}$. There was no signal for the mixture of 1,4-DHP and DMPO in the dark (Figure S5a in the Supporting Information). When the mixture was irradiated under light, there is a weak

DOI: 10.1021/acscatal.6b00879
ACS Catal. 2016, 6, 3365−3371

signal of DMPO-$O_2^{\bullet-}$ (Figure S5b). Interestingly, the signal of DMPO-$O_2^{\bullet-}$ was significantly enhanced after adding 1,4-DHP to the mixture (Figure S5c). Thus, the superoxide anion radical ($O_2^{-\bullet}$) was confirmed by ESR spectra (Figure S5), indicating that there is an obvious electron transfer of 1,4-DHP → C_3N_4 → O_2.

Figure 8b shows the mechanism of photocatalysis hydrogen evolution from 1,4-DHP, which is similar to the photooxidation mechanism, especially for the electron transfer of 1,4-DHP → C_3N_4. The electron transfer of 1,4-DHP → C_3N_4 from the ESR spectrum shows that the generation speed of holes in the VB with 1,4-DHP is slower than that without 1,4-DHP (Figure 8c,d), indicating electron transfer from 1,4-DHP to the CB of R-C_3N_4 after irradiation. Subsequently, there was electron transfer from the CB of R-C_3N_4 to the Pt salt. TEM images and XPS spectra of R-C_3N_4/Pt after the H_2 evolution reaction provides valuable information on the catalytically active species (Figure S6 in the Supporting Information). High-resolution XPS spectra of Pt 4f5/2 and Pt 4f7/2 from R-C_3N_4/$(NH_4)_2PtCl_6$ exhibit binding energies of 75.2 and 72 eV, respectively (Figure S6a), which is characteristic of Pt^0, suggesting that electron transfer from 1,4-DHP to R-C_3N_4 and $(NH_4)_2PtCl_6$ results in the reduction of $(NH_4)_2PtCl_6$ to Pt^0.[44−46] In order to confirm the existence of Pt^0 in the photocatalytic H_2 evolution reaction, high-resolution TEM (HRTEM) images of an R-C_3N_4/$(NH_4)_2PtCl_6$ sample after the H_2 evolution reaction were measured, as shown in Figure S6b. R-C_3N_4/Pt exhibits well-resolved lattice fringes with an interplanar spacing of 0.227 nm, which is believed to the (111) diffraction facet of pure Pt^0.[47] At the same time, 1,4-DHP transformed into the highly reactive 1,4-DHP cation radical, which is preferable for the release of H^+ and production of the final aromatization product **1b**, which were confirmed by the ^1H NMR, HRMS (Figures S7 and S8 in the Supporting Information), and HPLC spectra (Figure S9 in the Supporting Information).

Assessing the Defect Effects on the Photooxidation. In order to confirm and understand the structure−property relationship of defects, the cyano groups of mpg-C_3N_4 were reduced by $NaBH_4$, consequently converted into amino defects (see the Experimental Section).[36] To verify this conversion, the ninhydrin test was employed to measure the concentration of amino defects on the surfaces of these samples. As can be seen in Figure 4a, the reduced mpg-C_3N_4 shows an absorption intensity at 570 nm almost twice that of mpg-C_3N_4, indicating the cyano → amino conversion. Elemental analysis shows that the reduced mpg-C_3N_4 has more H content (3.88% H, Table S2 in the Supporting Information), which agrees with the results of the ninhydrin test. Then the photooxidation of 1,4-DHP was used to measure the photocatalytic ability of the modified mpg-C_3N_4. When the conversion of 1,4-DHP reached 99.9%, the reaction time was 50 min, which is 30 min shorter than that of mpg-C_3N_4 (Figure 4b). This indicates that the cyano defects greatly reduce the photocatalytic performance.

In addition, the amino defects of mpg-C_3N_4 were removed by a deamination reaction (see the Experimental Section). The absorption intensity of the ninhydrin test using deaminated mpg-C_3N_4 is almost two-thirds that of mpg-C_3N_4, and the H content reaches 3.16, indicating that some amino defects were indeed removed. The photooxidation ability of 1,4-DHP by deaminated mpg-C_3N_4 was slightly improved; the reaction time was 70 min as the product yield reached 99.9%. In comparison with amino defects, the cyano defects more greatly reduce the photocatalytic ability of mpg-C_3N_4. Moreover, this indicates that the improvement in photocatalysis ability mainly benefits from the defect repair.

CONCLUSION

In summary, through a facile and comprehensive copolymerization, a functionalized "little patch" (melamine) successfully remedies various defects of mesoporous carbon nitride, especially for the cyano and amino defects. When the weight ratio of melamine reaches 37.5%, R-C_3N_4 shows the least amount of defects and excellent electron−hole separation and transfer properties, which were confirmed by ESR, photocurrent, and conductivity measurements. R-C_3N_4 in the photoxidative aromatization of 1,4-DHP and H_2 evolution from 1,4-DHP not only meet the demand of sustainable chemistry but also offer another approach for H_2 production. H_2 evolution by R-C_3N_4 reaches 2700 μmol/g, and the turnover number is 2400, 6.5 times faster than that of mpg-C_3N_4. In an air atmosphere, the yield of the product reaches 99.5% after 40 min, which is almost 2 times higher than that of mpg-C_3N_4 and almost 5 times higher than that of g-C_3N_4. The effect of various defects on photooxidation was confirmed by chemical methods. This repair strategy offers new opportunities for developing the photocatalytic performance of carbon nitride.

ASSOCIATED CONTENT

Supporting Information

The Supporting Information is available free of charge on the ACS Publications website at DOI: 10.1021/acscatal.6b00879.

Additional experimental data including the SEM images, elemental analysis, XRD patterns, N_2 adsorption−desorption isotherms, UV−vis diffuse reflection spectra, VB (valence band) XPS, ESR spectra, and UV−vis absorption spectra of photooxidation of 1,4-DHP of prepared materials (PDF)

AUTHOR INFORMATION

Corresponding Authors

*E-mail for M.W.: wumb@upc.edu.cn.

*E-mail for H.Z.: zeng.haibo@njust.edu.cn.

Notes

The authors declare no competing financial interest.

ACKNOWLEDGMENTS

This work was financially supported by the National Basic Research Program of China (2014CB931700), the NSFC (61222403, 21302224, 51303212, 51372277, 51172285, and 51303202), the China Postdoctoral Science Foundation (2014M560590 and 2015T80758), the Shandong Provincial Natural Science Foundation (ZR2013BQ028 and ZR2013EMQ013), the Project of Science and Technology Program for Basic Research of Qingdao (14-2-4-47-jch), the Fundamental Research Funds for Central Universities (15CX05010A), and the State Key Laboratory of Fine Chemicals (KF1203).

REFERENCES

(1) Chen, C. C.; Ma, W. H.; Zhao, J. C. *Chem. Soc. Rev.* **2010**, *39*, 4206−4219.

(2) Xiang, Q. J.; Yu, J. G.; Jaroniec, M. *Chem. Soc. Rev.* **2012**, *41*, 782−796.

DOI: 10.1021/acscatal.6b00879
ACS Catal. 2016, 6, 3365−3371

(3) Liu, S. W.; Yu, J. G.; Jaroniec, M. *Chem. Mater.* **2011**, *23*, 4085−4093.
(4) Wu, W. T.; Geng, Y.; Fan, W. Y.; Li, Z. T.; Zhan, L. Y.; Wu, X. Y.; Zheng, J. T.; Zhao, J. Z.; Wu, M. B. *RSC Adv.* **2014**, *4*, 51349−51352.
(5) Wang, Y.; Wang, X. C.; Antonietti, M. *Angew. Chem., Int. Ed.* **2012**, *51*, 68−89.
(6) Wu, W. T.; Zhan, L. Y.; Fan, W. Y.; Song, J. Z.; Li, X. M.; Li, Z. T.; Wang, R. Q.; Zhang, J. Q.; Zheng, J. T.; Wu, M. B.; Zeng, H. B. *Angew. Chem., Int. Ed.* **2015**, *54*, 6540−6544.
(7) Wang, X. C.; Blechert, S.; Antonietti, M. *ACS Catal.* **2012**, *2*, 1596−1606.
(8) Zheng, Y.; Liu, J.; Liang, J.; Jaroniec, M.; Qiao, S. Z. *Energy Environ. Sci.* **2012**, *5*, 6717−6731.
(9) Mishra, Y. K.; Modi, G.; Cretu, V.; Postica, V.; Lupan, O.; Reimer, T.; Paulowicz, I.; Hrkac, V.; Benecke, W.; Kienle, L.; Adelung, R. *ACS Appl. Mater. Interfaces* **2015**, *7*, 14303−14316.
(10) Reimer, T.; Paulowicz, I.; Röder, R.; Kaps, S.; Lupan, O.; Chemnitz, S.; Benecke, W.; Ronning, C.; Adelung, R.; Mishra, Y. K. *ACS Appl. Mater. Interfaces* **2014**, *6*, 7806−7815.
(11) Su, D. S.; Zhang, J.; Frank, B.; Thomas, A.; Wang, X. C.; Paraknowitsch, J.; Schlogl, R. *ChemSusChem* **2010**, *3*, 169−180.
(12) Liu, J.; Liu, Y.; Liu, N. Y.; Han, Y. Z.; Zhang, X.; Huang, H.; Lifshitz, Y.; Lee, S.-T.; Zhong, J.; Kang, Z. H. *Science* **2015**, *347*, 970−974.
(13) Thomas, A.; Fischer, A.; Goettmann, F.; Antonietti, M.; Muller, J. O.; Schlogl, R.; Carlsson, J. M. *J. Mater. Chem.* **2008**, *18*, 4893−4908.
(14) Wang, Y.; Zhang, J. S.; Wang, X. C.; Antonietti, M.; Li, H. R. *Angew. Chem., Int. Ed.* **2010**, *49*, 3356−3359.
(15) Yan, S. C.; Li, Z. S.; Zou, Z. G. *Langmuir* **2009**, *25*, 10397−10401.
(16) Zhang, X. D.; Wang, H. X.; Wang, H.; Zhang, Q.; Xie, J. F.; Tian, Y. P.; Wang, J.; Xie, Y. *Adv. Mater.* **2014**, *26*, 4438−4443.
(17) Pawar, R. C.; Son, Y.; Kim, J.; Ahn, S. H.; Lee, C. S. *Curr. Appl. Phys.* **2016**, *16*, 101−108.
(18) Pawar, R. C.; Pyo, Y.; Ahn, S. H.; Lee, C. S. *Appl. Catal., B* **2015**, *176-177*, 654−666.
(19) Zhang, J. S.; Zhang, M. W.; Sun, R. Q.; Wang, X. C. *Angew. Chem., Int. Ed.* **2012**, *51*, 10145−10149.
(20) Chen, X. F.; Zhang, J. S.; Fu, X. Z.; Antonietti, M.; Wang, X. C. *J. Am. Chem. Soc.* **2009**, *131*, 11658−11659.
(21) Sun, J. H.; Zhang, J. S.; Zhang, M. W.; Antonietti, M.; Fu, X. Z.; Wang, X. C. *Nat. Commun.* **2012**, *3*, 1139−1146.
(22) Bai, X. J.; Wang, L.; Zong, R. L.; Zhu, Y. F. *J. Phys. Chem. C* **2013**, *117*, 9952−9961.
(23) Zhang, J. S.; Zhang, M. W.; Yang, C.; Wang, X. C. *Adv. Mater.* **2014**, *26*, 4121−4126.
(24) Zheng, Y.; Lin, L. H.; Ye, X. J.; Guo, F. S.; Wang, X. C. *Angew. Chem., Int. Ed.* **2014**, *53*, 11926−11930.
(25) Lin, Q. Y.; Li, L.; Liang, S. J.; Liu, M. H.; Bi, J. H.; Wu, L. *Appl. Catal., B* **2015**, *163*, 135−142.
(26) Shalom, M.; Inal, S.; Fettkenhauer, C.; Neher, D.; Antonietti, M. *J. Am. Chem. Soc.* **2013**, *135*, 7118−7121.
(27) Tang, J. W.; Durrant, J. R.; Klug, D. R. *J. Am. Chem. Soc.* **2008**, *130*, 13885−13891.
(28) Martin, D. J.; Qiu, K. P.; Shevlin, S. A.; Handoko, A. D.; Chen, X. W.; Guo, Z. X.; Tang, J. W. *Angew. Chem., Int. Ed.* **2014**, *53*, 9240−9245.
(29) Goettmann, F.; Fischer, A.; Antonietti, M.; Thomas, A. *Angew. Chem., Int. Ed.* **2006**, *45*, 4467−4471.
(30) Cui, Y. J.; Zhang, G. G.; Lin, Z. Z.; Wang, X. C. *Appl. Catal., B* **2016**, *181*, 413−419.
(31) Tay, Q.; Kanhere, P.; Ng, C. F.; Chen, S.; Chakraborty, S.; Huan, A. C. H.; Sum, T. C.; Ahuja, R.; Chen, Z. *Chem. Mater.* **2015**, *27*, 4930−4933.
(32) Zhang, J. S.; Zhang, G. G.; Chen, X. F.; Lin, S.; Mohlmann, L.; Dolega, G.; Lipner, G.; Antonietti, M.; Blechert, S.; Wang, X. C. *Angew. Chem., Int. Ed.* **2012**, *51*, 3183−3187.
(33) Du, A. J.; Sanvito, S.; Li, Z.; Wang, D. W.; Jiao, Y.; Liao, T.; Sun, Q.; Ng, Y. H.; Zhu, Z. H.; Amal, R.; Smith, S. C. *J. Am. Chem. Soc.* **2012**, *134*, 4393−4397.
(34) Zhang, D.; Wu, L. Z.; Zhou, L.; Han, X.; Yang, Q. Z.; Zhang, L. P.; Tung, C. H. *J. Am. Chem. Soc.* **2004**, *126*, 3440.
(35) Wu, P.; Wang, J. R.; Zhao, J.; Guo, L. J.; Osterloh, F. E. *J. Mater. Chem. A* **2014**, *2*, 20338−20344.
(36) Hothi, P.; Hay, S.; Roujeinikova, A.; Sutcliffe, M. J.; Lee, M.; Leys, D.; Cullis, P. M.; Scrutton, N. S. *ChemBioChem* **2008**, *9*, 2839−2845.
(37) Chu, S. Y.; Wang, Y.; Guo, Y.; Feng, J. Y.; Wang, C. C.; Luo, W. J.; Fan, X. X.; Zou, Z. G. *ACS Catal.* **2013**, *3*, 912−919.
(38) Jürgens, B.; Irran, E.; Senker, J.; Kroll, P.; Müller, H.; Schnick, W. *J. Am. Chem. Soc.* **2003**, *125*, 10288−10300.
(39) Lin, Z. Z.; Wang, X. C. *Angew. Chem., Int. Ed.* **2013**, *52*, 1735−1738.
(40) Xu, J.; Zhang, L. W.; Shi, R.; Zhu, Y. F. *J. Mater. Chem. A* **2013**, *1*, 14766−14772.
(41) Yang, S. B.; Gong, Y. J.; Zhang, J. S.; Zhan, L.; Ma, L. L.; Fang, Z. Y.; Vajtai, R.; Wang, X. C.; Ajayan, P. M. *Adv. Mater.* **2013**, *25*, 2452−2456.
(42) Field, A.; Field, J. *Food Chem.* **2010**, *121*, 912−917.
(43) Chen, D. M.; Wang, K. W.; Xiang, D. G.; Zong, R. L.; Yao, W. Q.; Zhu, Y. F. *Appl. Catal., B* **2014**, *147*, 554−561.
(44) Li, Q.; Cui, C.; Meng, H.; Yu, J. G. *Chem. - Asian J.* **2014**, *9*, 1766−1770.
(45) Petit, C.; Seredych, M.; Bandosz, T. J. *J. Mater. Chem.* **2009**, *19*, 9176−9185.
(46) Chen, D. H.; Zhao, Y. C.; Fan, Y. F.; Peng, X. L.; Wang, X.; Tian, J. N. *J. Mater. Chem. A* **2013**, *1*, 13227−13232.
(47) Yang, W. H.; Wang, H. H.; Chen, D. H.; Zhou, Z. Y.; Sun, S. G. *Phys. Chem. Chem. Phys.* **2012**, *14*, 16424−16432.

DOI: 10.1021/acscatal.6b00879
ACS Catal. 2016, 6, 3365−3371